IEEE Access
Multidisciplinary | Rapid Review | Open Access Journal

Received 12 March 2024, accepted 17 March 2024, date of publication 21 March 2024, date of current version 1 April 2024.

Digital Object Identifier 10.1109/ACCESS.2024.3380463

RESEARCH ARTICLE

Evaluation of Mechanical Properties Considering Uncertainties for Hairpin Coils in Electric Vehicle Motor Manufacturing

YOUNG-DAE SHIM[1], JIHUN KIM[2], CHANGHYEON KIM[2], JIHYUN PARK[3], DONG-WOOK YANG[3], AND EUN-HO LEE[1,4,5]

[1]Department of Smart Fabrication Technology, Sungkyunkwan University, Suwon-si 16419, Republic of Korea
[2]Department of Mechanical Engineering, Sungkyunkwan University, Suwon-si 16419, Republic of Korea
[3]Data Science Team, Hyundai Mobis, Seoul 06141, Republic of Korea
[4]School of Mechanical Engineering, Sungkyunkwan University, Suwon-si 16419, Republic of Korea
[5]Department of Intelligent Robotics, Sungkyunkwan University, Suwon-si 16419, Republic of Korea

Corresponding author: Eun-Ho Lee (e.h.lee@skku.edu)

This work was supported by the Data Science Team, Hyundai Mobis Company Ltd.

ABSTRACT The rising demand for electric vehicles (EVs) underscores the need for enhancing electric motor efficiency. Utilizing hairpin coils with a rectangular cross-section has emerged as an alternative approach to increase conductor density in motor stator slots. However, the manufacturing process for hairpin coil motors presents challenges such as springback, which stems from wire shaping processes such as leveling and bending with plastic deformation. These challenges are closely tied to mechanical properties of the Young's modulus and yield stress. This study investigates uncertainties in mechanical property evaluation using a combination of tensile tests, analytic solutions, numerical simulations, and a present double-sided four-point bending method. The results show significant variations in the Young's modulus, which affect the determination of yield stress in tensile tests. It has been revealed that in order to obtain stable mechanical properties of hairpin coils in tensile tests, the conditions should be restricted to a very slow strain rate, slower than 10^{-3} s^{-1}. To address this, this study introduces an alternative method that combines double-sided four-point bending and tensile tests, allowing for the acquisition of Young's modulus without prior information on material properties. This approach reduces uncertainties in determination of the mechanical properties with much less time cost.

INDEX TERMS Hairpin winding motor, springback, tensile tests, double-sided four-point bending, Young's modulus, yield stress.

I. INTRODUCTION

The rising demand for electric vehicles (EVs) in the automotive industry has driven a shift in the primary components from internal combustion engines to electric motors. In an EV, an electric motor drives the magnetic field from a stator to cause the rotation of a rotor, which is composed of a permanent magnet. The generation of this magnetic field is facilitated by copper wires within the stator slot [1]. The limitations on the magnetic field due to shape factor constraints addressed through the use of hairpin coils, which is characterized by a rectangular cross-sectional geometry [2], [3], [4]. Hairpin coils help mitigate the impact of the stator slot geometry by minimizing empty space while simultaneously enhancing the winding number and magnetic field strength, as shown in Fig. 1a. Hairpin coils are produced by incorporating additional manufacturing processes involving straightening and bending oxygen-free high-conductivity (OFHC) copper wires [5], as shown in Fig. 1b. These additional processes result in plastic deformation of the material, the resistivity of the conductor increases which leads to AC loss and influences the performance for traction drives [6], [7]. Moreover, the plastic deformation causes common metal-forming quality

The associate editor coordinating the review of this manuscript and approving it for publication was Amin Mahmoudi.

issue such as springback. Specifically, after bending the coil, it is inserted into the designated slots of the stator to produce the motor. However, during this process, shape change due to springback (elastic recovery) after bending often causes difficulties in fitting the coil into the stator slots, resulting in alignment issues and assembly challenges. This quality issue is closely tied to the current state of the material mechanical properties. In particular, Young's modulus and yield strength are critical mechanical properties that directly influence the magnitude of springback after metal forming [8], [9]. Consequently, to improve the quality of hairpin winding motors, the mechanical properties of the hairpin coils must be considered to optimize the forming process. Typically, the process conditions of the manufacturing line remain constant during the production of products with identical dimensions. However, the mechanical properties may vary between suppliers, lot numbers, and even the length direction within the same bobbin [10]. Such property deviations contribute to springback issues that result in failures when the manufactured hairpins are inserted into the stator slot [11], [12]. It is therefore crucial to maintain consistency in the mechanical properties of the hairpin coils through regular mechanical property assessments during the manufacturing process. Because this is not a significant concern in conventional motor coils [8], [13], [14], [15], there have been few reports on evaluating the mechanical properties of hairpin coils.

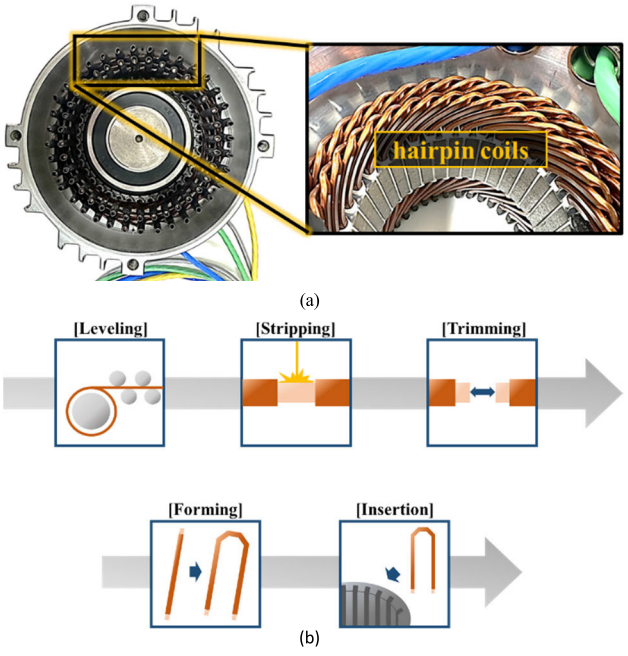

FIGURE 1. Hairpin coil winding motor: (a) Stator of a hairpin coil winding motor and (b) the schematic of the hairpin coil forming process.

Although previous studies have been conducted on the metallurgical effects of copper wires on their mechanical properties, the reliability of the specific test conditions and methods were not addressed in these studies [16], [17], [18], [19], [20], [21]. The mechanical properties of the copper wires in these studies were measured using universal tensile machines (UTMs). There is a need to improve the standardization of the strain rates and specimen lengths because a wide range of test conditions have been applied with specimen lengths ranging from 50 to 150 mm and strain rates from 1.67×10^{-4} to 5×10^{-3} s^{-1}. The outcomes obtained under these test conditions have not been validated to be representative of the precise material properties of the copper wire. Moreover, unlike the observed deformation of a dog-bone-shaped specimen, the deformation in a hairpin coil is not concentrated within the specified gauge length because of limitations imposed by the wire geometry. Consequently, the measured stress values do not precisely reflect the deformation response in the specified gauge section. An accurate setting of the gauge length holds significant importance in calculating strain and determining Young's modulus. Additionally, the hairpin coil is a material in composite form. A polymer-based insulator material is coated on the copper conductor surface. This insulator significantly affects the experimental results of the tensile tests [11], [22]. The forming conditions are based on the combined properties of the insulator and conductor. An approach using the nanoindentation method to identify the Young's modulus of the insulator has been conducted [13], [23]. The mechanical properties were obtained by the FEM inverse method, optimizing the material model parameters to coincide with the experimental data. In particular, the reported Young's moduli of hairpin coils in a previous study range from 84 to 98 GPa [10], [22]. Even though the applied strain rate of the tensile test is considered to be under static conditions, the elastic property varies widely. This variation significantly affects the calculation of the yield strength from the slope change in the 0.2% offset method. Therefore, a thorough investigation is required to evaluate the mechanical properties of hairpin coils.

The aim of this study is to comprehensively evaluate the Young's modulus and yield strength of insulated copper wire used in hairpin coil manufacturing. For this purpose, the main study content consists of three major components: (1) observing uncertainties arising from the conditions of tension tests, (2) optimizing tension test conditions to eliminate uncertainties, and (3) presenting a double-sided four-point bending test to complement tension tests. Initially, tensile tests were conducted under controlled length and strain rate conditions to assess the variations in the Young's modulus. The test results revealed uncertainties in the measured values of the mechanical properties that varied with the tensile test conditions. The Young's modulus was strongly influenced by the experimental conditions. These variations have corroborated the results reported in a previous study [7] on the properties of hairpin coils. Furthermore, the significant influence that the Young's modulus has on determination of the yield strength is a contributing reason for the variation in the properties of hairpin coils in the industry. In the second topic, to optimize hairpin motor manufacturing and

improve quality control, it is essential to establish criteria for obtaining stable mechanical properties for the industry. While the test results show that stable values of the Young's modulus can be obtained by performing tensile tests at very low strain rates, the industrial preference often tends to avoid conducting tensile tests on long hairpin coils with low strain rates due to the extended duration required for such experiments. For the last assessment, to mitigate uncertainties and obtain stable mechanical properties, a double-sided four-point bending test is presented as an alternative to the tensile test for measuring the Young's modulus. This method allows the Young's modulus of the hairpin coil to be measured without information of the individual properties of copper or insulation in advance, thereby reducing the uncertainty associated with the information. Consistent stable values were obtained from the four-point bending test without damaging the specimen even within short testing durations, based on a new hybrid methodology that integrates four-point bending and tensile tests. The former was employed for the Young's modulus measurements, while the latter was used to obtain a stress-strain curve within the plastic region for yield strength measurements. The hybrid approach was validated through precisely controlled tensile and indentation tests and its ability to effectively provide stable mechanical properties.

The remainder of this paper is structured as follows: Section II presents the tensile test results with the variation of Young's modulus observed during the tensile tests. Section III introduces the double-sided four-point bending method for Young's modulus measurements, which achieved stable measurement results compared to those of the tensile tests. Section IV presents the yield strength and elastic recovery calculation accuracy of the proposed method compared to the conventional conditions. Section V provides a comprehensive discussion of the results, and Section VI concludes the paper.

II. EXPERIMENTAL AND NUMERICAL INVESTIGATION OF TENSILE TEST CONDITION

OFHC copper was used for the hairpin coil material. Compared with regular copper, OFHC copper is an enhanced product in which oxygen and other impurities in the material are limited below 10 ppm to improve its electrical conductivity and mitigate hydrogen embrittlement. Notably, it is widely used in electronic devices owing to its superior conductivity and electrical efficiency. A layer of insulating material (polyamide-imide) is coated onto the surface of copper wires to prevent the formation of closed circuits from contact between the wires. The insulating material is applied by immersing preheated copper wire in a liquid insulating resin and curing it in a dryer. The insulator thickness of the copper wire in the samples used in this study is 114 μm.

A hairpin coil comprises a copper wire coated with an insulator. It is thus a composite material with two distinct components. The stress-strain curve encompasses the properties of both the copper wire and insulator, dependent on their cross-sectional area ratio. The Young's modulus can be calculated using the rule of mixtures, a common approach in composite materials analysis [24], [25].

$$A_{\mathrm{H}} \cdot \sigma_{\mathrm{H}} = A_{\mathrm{C}} \cdot \sigma_{\mathrm{C}} + A_{\mathrm{I}} \cdot \sigma_{\mathrm{I}}, \tag{1a}$$

where $A_{\mathrm{H}} = A_{\mathrm{C}} + A_{\mathrm{I}}$,

$$E_{\mathrm{H}}^{\mathrm{T}} \varepsilon_{\mathrm{H}} = \alpha \cdot E_{\mathrm{C}} \varepsilon_{\mathrm{C}} = (1-\alpha) \cdot E_{\mathrm{I}} \varepsilon_{\mathrm{I}}, \tag{1b}$$

where $\alpha = A_{\mathrm{C}}/A_{\mathrm{H}}$,

$$E_{H}^{\mathrm{T}} = \alpha \cdot E_{\mathrm{C}} + (1-\alpha) \cdot E_{\mathrm{I}}. \tag{1c}$$

In the above equation, A is the cross-sectional area of each material and σ denotes the stress applied to each material. The Young's modulus and strain are denoted by E and ε, respectively. The subscripts H, C, and I denote the hairpin, copper, and insulator, respectively. The superscript T in $E_{\mathrm{H}}^{\mathrm{T}}$ denotes the Young's modulus obtained from tensile test. Equation (1a) is the force equilibrium equation for the composite while in (1b), each force component is expressed in terms of Young's modulus and strain. Under the assumption no slipping occurs within the individual materials of the composite structure so that ε_{H}, ε_{C}, and ε_{I} have the same values, the Young's modulus of the composite is given by (1c).

The geometric constraints on the copper wire make it difficult to fabricate the specimen into a dog-bone shape. Consequently, the average strain over the entire length is used. The strain is given by the following equation.

$$\varepsilon = \int_{l_o}^{l} \frac{1}{l} \mathrm{d}l = \ln(\frac{l}{l_o}) = \ln(\lambda). \tag{2}$$

In the above equation, l_0 is the initial length of the sample, l denotes the length after deformation, and λ denotes the mechanical stretch ratio. Because the insulated copper wire does not have a specific gauge length, the stretched length was defined as the cross-head displacement under the assumption that there is no slippage between the test grip and sample.

Before conducting tensile tests, a numerical simulation was performed to assess the validity of evaluating the mechanical properties of the hairpin coil through tensile tests. Finite element (FE) simulations were conducted using the Abaqus software (Dassault Systèmes, France). The hairpin coil geometry was modeled in a three-dimensional domain with a copper thickness of 1.44 mm and width of 3.06 mm, and a 0.114 mm thick insulator layer was modeled on its outer surface. The overall length of the sample was 350 mm. The contact condition between the copper wire and the insulator was disregarded based on the assumption that there was no slip as described in (1). A Z-axis symmetry condition was applied to the lower surface, and X- and Y- axis symmetry conditions to the left and front surfaces, respectively, to reduce computational time and prevent translational motion. The wire was partitioned at 30 mm and constrained by a reference point for the grip region, and a velocity condition of 0.003 mm/s along the Z-direction was

set to apply tension on the specimen. Further details of the boundary conditions are presented in Fig. 2a.

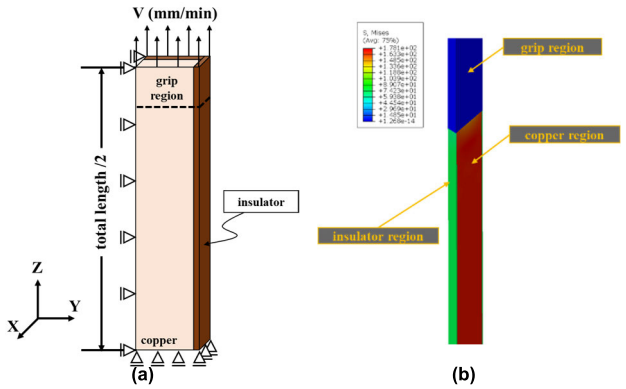

FIGURE 2. Tensile simulation boundary conditions and results: (a) Boundary conditions and (b) stress distribution in individual materials.

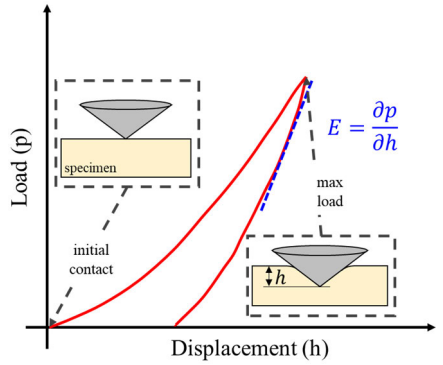

FIGURE 3. Nanoindentation method for Young's modulus measurement.

TABLE 1. Simulation properties for hairpin coil.

Property	Copper	Insulator
Elastic properties		
Young's modulus [GPa]	112.4	3.5
Strain hardening		
A [MPa]	117	-
B [MPa]	239	
n [-]	0.36	
C [28]	0.025	0

In the FE simulation, the material properties are shown in Table 1. The Young's modulus values for each material were experimentally determined through the indentation method, as depicted in Fig. 3. General Johnson-Cook model was used for modeling plasticity for copper, and insulator was assumed to be perfect-plastic material which yields at 75 MPa [13], [26]. Because only the strain hardening effect was considered for this study, the rate hardening and temperature softening terms were neglected. Only the experimental and reference values are presented here given that the primary focus of this paper is on the tensile and four-point bending methods. The plastic deformation calculations were performed using an isotropic yield function based on the associated flow rule [27].

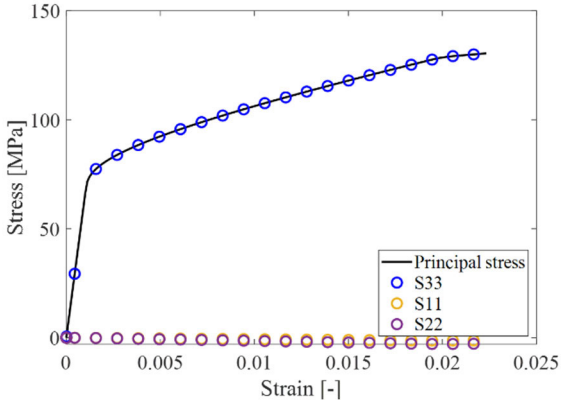

FIGURE 4. Stress-strain curve of the tensile simulation.

The stress distributions in the simulation results are shown in Fig. 2b. Because the specimen has a wire shape and is composed of two materials with distinct properties, it is necessary to confirm that of uniaxial tension was indeed achieved under the imposed boundary conditions. The stress components derived from the simulation results are presented in Fig. 4. A comparative analysis was conducted on the principal stress and stresses along the Z-, X-, and Y- directions as the strain increases. The stress values were extracted from elements on the Z-symmetry plane. Subsequently, the average stresses of the elements within each material were computed, and the total stress of the hairpin structure was determined by using each material cross-sectional area proportions in a similar manner to (1c). The results show that the stress in the Z-direction is aligned with the maximum principal stress. In contrast, the stress components along the X- and Y- directions are close to zero. This validation confirms that the hairpin coil was subjected to uniaxial tension under the current applied boundary conditions and that the mechanical properties of hairpin coils can theoretically be determined from tensile tests.

The Young's moduli from the tensile simulation results were compared with the analytically calculated values by (1). The computed slope of the linear region in the stress-strain curve corresponds to 91 GPa, which closely mirror the value of 88.4 GPa estimated using (1c). The mechanical properties obtained from indentations tests listed in Table 1 were used to obtain the Young's moduli of the hairpin coil in both the analytical expression and FE simulation. The similarity of the Young's moduli obtained using the three methods serves as a cross-validation of their validity. This suggests that actual tensile experiments on hairpin coils should yield similar results.

In addition, the undeformed length was determined before the tensile test case studies. The difficulty of concentrating

the deformation in a hairpin coil at the gauge length during tensile testing can cause the experimental results to be affected by uneven deformation in the grip portion [29]. Note that a specific length portion within the grip section does not contribute to tensile deformation. As the strain is calculated by considering the average length change across the entire specimen, it is imperative that the length of the undeformed portion is subtracted from the total specimen length. The tested samples yield consistent values for the Young's modulus, which is a function of only the material microstructure and not the specimen length. The effective strain derived from the tensile test results has been calculated as follows.

$$\varepsilon_{\mathrm{n}} = \frac{L'}{L_0^{\mathrm{n}}} - \beta, \quad \text{where n} = 1 - 4. \tag{3}$$

Here, L' represents the length change, L_0 denotes the initial specimen length, and β denotes for an effective undeformed length affected by experimental conditions, such as that due to the grip length. The subscript and superscript n represent the different specimen lengths. The Young's modulus of the hairpin in the tensile test was determined from the slope in the linear region of the stress-strain curve. The cross-head speed V_{C} of the UTM was set as

$$V_C = 60 \cdot \dot{\varepsilon} \cdot L_g^n (\mathrm{mm/min}), \quad \text{where } L_{\mathrm{g}}^{\mathrm{n}} = L_0^{\mathrm{n}} - \beta. \tag{4}$$

In the above equation, $L_{\mathrm{g}}^{\mathrm{n}}$ is the initial length of the gauge length which is defined as $L_0^{\mathrm{n}} - \beta$ in (3). The constant 60 is positioned to make the unit of speed into mm/min. Here, the cross-head speed of the UTM was controlled by setting the undeformed length β to 0 mm and the strain rate to 10^{-4} s^{-1}. Despite the variation in strain rate from its inherent value, it remains consistent across different specimen lengths. For the determination of effective undeformed length, β is systematically adjusted from 0 – 100 mm to investigate the Young's modulus variation between each specimen length. The specimen wires were gripped by two grips, with the grip region fixed at 30 mm on each end of the specimen. The bottom grip was fixed, while the top grip was attached to the moving cross-head to conduct the uniaxial tensile test, as shown in Fig. 5(a). The lengths of the specimens were set to 220 mm, 270 mm, 320 mm, and 370 mm for each condition, while the dimensions of the cross-section were fixed at 3.26 mm × 1.67 mm for every specimen, as shown in Fig. 5 (b).

The calculated results and standard deviations of $E_{\mathrm{H}}^{\mathrm{T}}$ are shown in Fig. 6. Figure 6a shows that the Young's modulus $E_{\mathrm{H}}^{\mathrm{T}}$ decreased as the undeformed length β increased. This decrease is attributed to the increased strain values despite the constant amount of deformation. The change of the Young's modulus also trends concerning the total specimen length, indicating a substantial impact of the β parameter on shorter specimens. Figure 6b shows the variation of the $E_{\mathrm{H}}^{\mathrm{T}}$ deviation according to specimen length in relation to the β parameter. The deviation decreased as β increases up to 27 mm and then experiences an upturn. The calculation

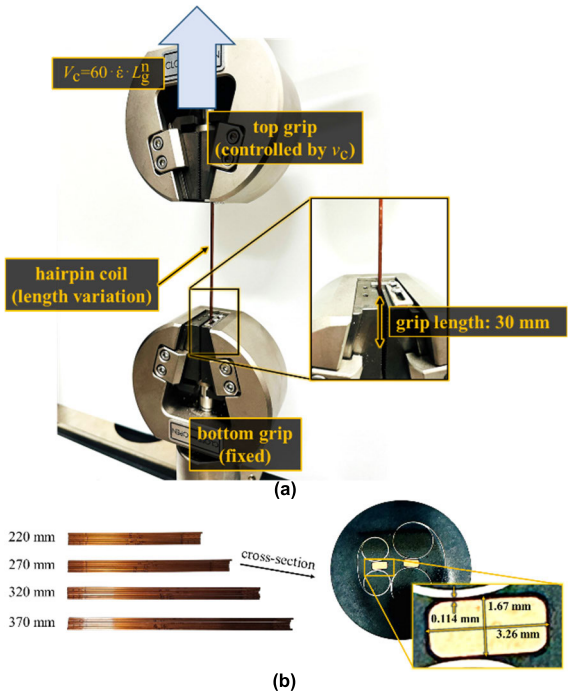

FIGURE 5. Experimental setup of the tensile test for hairpin coil; (a) picture of the specimen mounted UTM and (b) hairpin coil specimen preparation with length variation.

results shows that the undeformed length of approximately 27 mm reduces the deviation, which demonstrates the appropriateness of using (3) when calculating strain for different length specimens. The determined value can be used for the specified grip length and shape used in this study, but the calculation must be repeated for different grip conditions.

Based on the above discussions, tensile tests were conducted to confirm the variations in the Young's modulus of hairpin coils. The specimen lengths were set to 220, 270, 320, and 370 mm, which corresponds to the β determination experiments conducted previously. Tensile tests were conducted at the six different strain rates of 10^{-1}, 10^{-2}, 5×10^{-3}, 10^{-3}, 10^{-4} and 10^{-5} s^{-1} resulting a total of 24 experimental cases. The cross-head speed of the UTM was set using (4). The resultant stress-strain curves from the tensile tests are presented in Fig. 7. These curves are categorized based on the strain-rate dependency. As the strain rate increased, it can be observed that the slopes in the elastic range of the stress-strain curves varied depending on the lengths of the specimens. When the strain rate increases from 10^{-5} s^{-1} to 10^{-1} s^{-1}, the Young's modulus values exhibit a significant variation from 20 GPa to 90 GPa. A strain rate of 10^{-1} s^{-1} is typically not considered as high strain rate range for metallic materials. Therefore, the experimental results confirm the need for careful consideration in setting the strain rate for measuring the mechanical properties of hairpin coil motors. The measured Young's modulus according to the experimental conditions are illustrated in Fig. 8. For strain

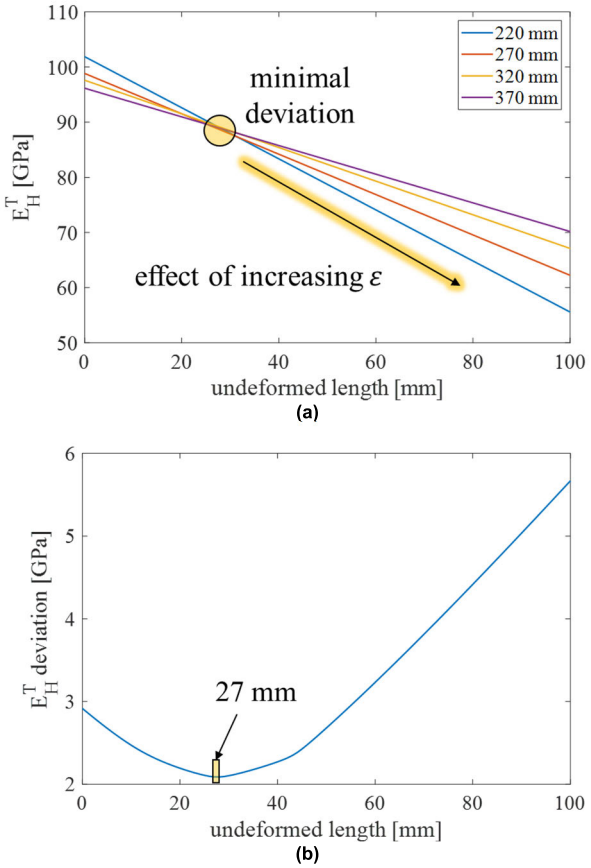

FIGURE 6. Undeformed length effect on Young's modulus calculation; (a) Calculated E_H^T according to undeformed length β β and (b) Average standard deviation of E_H^T according to β.

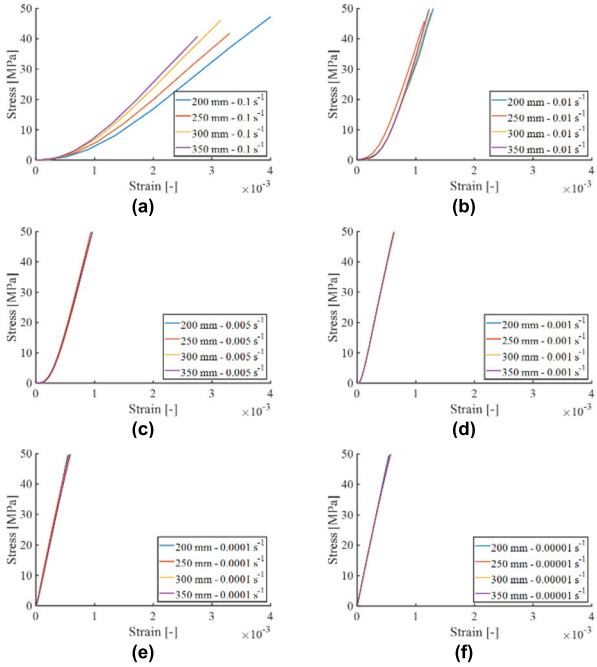

FIGURE 7. Stress-strain curves in elastic region of tensile tests; (a) $\dot{\varepsilon} = 10^{-1}$ s^{-1}; (b) $\dot{\varepsilon} = 10^{-2}$ s^{-1}; (c) $\dot{\varepsilon} = 5 \times 10^{-3}$ s^{-1}; (d) $\dot{\varepsilon} = 10^{-3}$ s^{-1}; (e) $\dot{\varepsilon} = 10^{-4}$ s^{-1} and (f) $\dot{\varepsilon} = 10^{-5}$ s^{-1}.

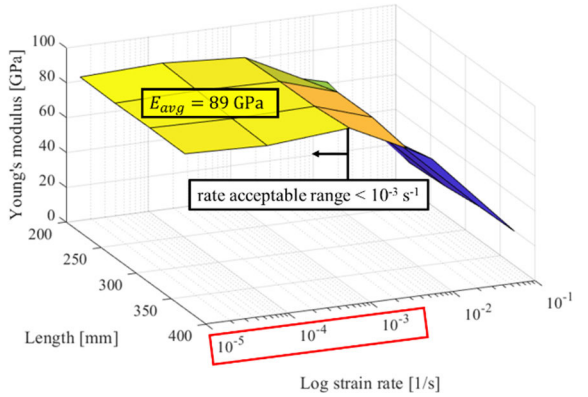

FIGURE 8. Change of tensile Young's modulus according to specimen length and strain rate.

rates below 10^{-3} s^{-1}, the Young's modulus was consistently measured approximately 89 GPa regardless of the specimen length. This value is consistent with the FE simulation and analytic calculation results presented in Table 2. In addition, the Young's moduli obtained fall within an acceptable range, matching those of previous experimental studies [22]. However, the provided results of the Young's moduli in the study only show the variation of the property measured under a 10^{-4} s^{-1} strain rate condition; therefore, the rate-dependent uncertainty is not considered. It is recommended that the properties of hairpin coils be measured at strain rates below 10^{-3} s^{-1}.

TABLE 2. Analytical and simulation results of Young's modulus calculation.

Test method	Analytical [GPa]	Simulation [GPa]
Tensile test	88.4	91.0

However, conducting tensile tests on specimens with a length of 300 mm at a strain rate of 10^{-3} s^{-1} results in an extremely slow testing speed. This test condition is therefore not preferred in the industrial applications. In this study, we present an alternative method in which double-sided four-point bending test is combined with tensile test to obtain stable values for the Young's modulus and yield strength.

III. DOUBLE-SIDED FOUR-POINT BENDING

The four-point bending test specified in ASTM D6272-17 is a standardized method for determining the Young's or flexural moduli of composites or insulated wire products. This method involves placing a sample on two supports measuring the downward displacement when a load is applied with two noses. The schematic of the four-point bending test is shown in Fig. 9. The ratio of the span distance between the supports to the distance between the noses is typically set to 2:1 or 3:1.

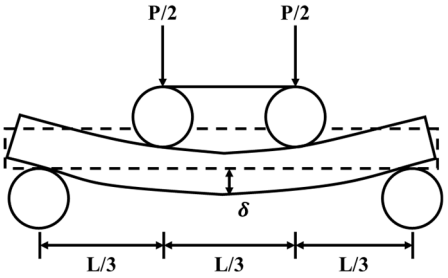

FIGURE 9. Schematic of the four-point bending test method.

A 3:1 ratio was employed in this test. The four-point bending test method facilitates the application of pure bending to the material by eliminating shear stresses in the section where the displacement is measured under a load. However, measuring the Young's modulus of hairpin coil using traditional four-point bending requires the Young's modulus information of insulator in advance to obtain the OFHC copper property. This limitation makes it industrially less feasible. A double-sided four-point bending method to evaluate the Young's moduli of hairpin coils without prior information on the insulator property is presented in this paper.

The strain, stress, and moment of the specimens under pure bending can be calculated as follows:

$$\varepsilon_{\mathrm{x}} = -\frac{y}{\rho}, \tag{5a}$$

$$\sigma_{\mathrm{x}} = -E_{\mathrm{H}}^{\mathrm{B}}\frac{y}{\rho}, \tag{5b}$$

$$M = \frac{E_{\mathrm{H}}^{\mathrm{B}}}{\rho}\int y^2 \mathrm{d}A = \frac{E_{\mathrm{H}}^{\mathrm{B}} I}{\rho}. \tag{5c}$$

ρ is the radius of curvature and y is the distance from the neutral axis of the specimen. The superscript B in $E_{\mathrm{H}}^{\mathrm{B}}$ denotes the bending test. In (5c), I is the area moment of inertia of the specimen, which is calculated as $bh^3/12$ for a rectangular geometry. Although the moment in the beam can be calculated using (5c), the practical challenges of experimentally measuring the radius of curvature in (5c) make it necessary to replace the radius of curvature with the deflection caused by the four-point bending test. The curvature is defined as follows:

$$\mathrm{d}s = \rho \mathrm{d}\theta, \tag{6a}$$

$$\mathrm{d}s = \sqrt{\mathrm{d}x^2 + \mathrm{d}v^2} = \sqrt{1 + (\mathrm{d}v/\mathrm{d}x)^2}\cdot \mathrm{d}x, \tag{6b}$$

$$(1 + \tan^2\theta)\mathrm{d}\theta = \frac{d^2v}{\mathrm{d}x^2}\cdot \mathrm{d}x, \quad \text{where } \tan\theta = \frac{\mathrm{d}v}{\mathrm{d}x}. \tag{6c}$$

In the above equations, v is the specimen deflection caused by bending, and x the displacement along the longitudinal direction of the specimen. The curvature length ds is defined through (6a) and (6b). Additionally, the central angle $\mathrm{d}\theta$ can be expressed in terms of the deflection and the displacement along the x-direction via (6). Substituting (6) into (6a) and employing (6b), yields the following expressions:

$$\rho \cdot \frac{(\frac{\mathrm{d}^2v}{\mathrm{d}x^2})\cdot \mathrm{d}x}{1 + (\frac{\mathrm{d}v}{\mathrm{d}x})^2} = \mathrm{d}s = \sqrt{1 + (\frac{\mathrm{d}v}{\mathrm{d}x})^2}\cdot \mathrm{d}x, \tag{7a}$$

$$\rho = [1 + (\frac{\mathrm{d}v}{\mathrm{d}x})^2]^{3/2}\cdot\frac{\mathrm{d}x^2}{\mathrm{d}^2v} \approx \frac{\mathrm{d}x^2}{\mathrm{d}^2v}, \tag{7b}$$

$$E_{\mathrm{H}}^{\mathrm{B}} = \frac{M}{I}\cdot\frac{\mathrm{d}x^2}{\mathrm{d}^2v}. \tag{7c}$$

Because the deflection angle is exceptionally small during elastic deformation, higher-order terms in the deflection angle in (7b) can be disregarded. Consequently, the radius of curvature can be expressed as the reciprocal of the second derivative of the deflection. Using (7a) and (7b), the Young's modulus in the bending test can be expressed as a function of the bending moment, area moment of inertia, and second derivative of deflection in (7c).

The following expressions are used to derive the Young's modulus of the hairpin coil in the bending test, in which the deflection is measured at the center of the specimen:

$$v(x) = \frac{1}{12E_{\mathrm{H}}^{\mathrm{B}}I}PLx^2 - \frac{1}{36E_{\mathrm{H}}^{\mathrm{B}}I}PL^2x + \frac{1}{324}PL^3, \tag{8a}$$

$$v(\frac{1}{2}L) = \delta = 0.21\frac{PL^3}{E_{\mathrm{H}}^{\mathrm{B}}I}, \tag{8b}$$

$$E_{\mathrm{H}}^{\mathrm{B}} = 0.21\cdot\Delta\frac{L^3}{bh^3}. \tag{8c}$$

The deflection within the $1/3L < x < 2/3L$ region is defined in (8a). Because the deflectometer measurement is performed at the center of the specimen during the bending test, the total deflection at the center is calculated using (8b). By rearranging the terms in (8b), the bending Young's modulus of the hairpin coil can be expressed through (8c). In this equation, Δ is the slope of the load-deflection curve in the elastic region while b and h are the width and thickness of the specimen, respectively.

The total bending stiffness of the hairpin coil composite structure can be expressed as the sum of the bending stiffnesses of each material [30]:

$$E_{\mathrm{H}}^{\mathrm{B}}I = E_{\mathrm{C}}I_{\mathrm{C}} + E_{\mathrm{I}}I_{\mathrm{I}}. \tag{9}$$

In the above equation, I_{C} and I_{I} are the area moments of inertia of copper and the insulator, respectively. Although the bending modulus of the hairpin coil can be determined in a single test without distinguishing the copper and insulator components, challenges in the conversion of the bending modulus into the tensile modulus. At least one of the individual material properties must be provided to perform the conversion. Equation (9) can be transformed to obtain the Young's moduli of the individual materials from the results of a double-sided four-point bending test.

$$\begin{aligned} E_{\mathrm{H},1}^{\mathrm{B}}I_{\mathrm{H},1} &= E_{\mathrm{C}}I_{\mathrm{C},1} + E_I I_{\mathrm{I},1}, \\ E_{\mathrm{H},2}^{\mathrm{B}}I_{\mathrm{H},2} &= E_{\mathrm{C}}I_{\mathrm{C},2} + E_I I_{\mathrm{I},2}, \end{aligned} \tag{10a}$$

$$E_C = \left(\frac{E^B_{H,1} I_{H,1}}{I_{I,1}} - \frac{E^B_{H,2} I_{H,2}}{I_{I,2}}\right) / \left(\frac{I_{C,1}}{I_{I,1}} - \frac{I_{C,2}}{I_{I,2}}\right),$$
$$E_I = \left(\frac{E^B_{H,1} I_{H,1}}{I_{C,1}} - \frac{E^B_{H,2} I_{H,2}}{I_{C,2}}\right) / \left(\frac{I_{I,1}}{I_{C,1}} - \frac{I_{I,2}}{I_{C,2}}\right). \quad (10b)$$

In the above equations, $I_{H,1}$ and $I_{H,2}$ are the area moments of inertia of the hairpin coil when subjected to a four-point bending test along the thickness and width directions, respectively. Owing to the non-square cross-sectional shape of the copper wire used in the hairpin, the area moments of inertia differs when the load is applied along the thickness and width directions. This results in two distinct equations derived from the double-sided four-point bending tests. The Young's modulus of each individual material can be determined using (10b). The tensile Young's modulus of the hairpin coil can then be converted from the bending modulus using the outcomes the Young's moduli of the individual materials and (1c). Notably, the reliability of the results from theses equations is enhanced by their derivation from the existing bending test standards for composites. The schematic of the double-sided four-point bending test is depicted in Fig. 10.

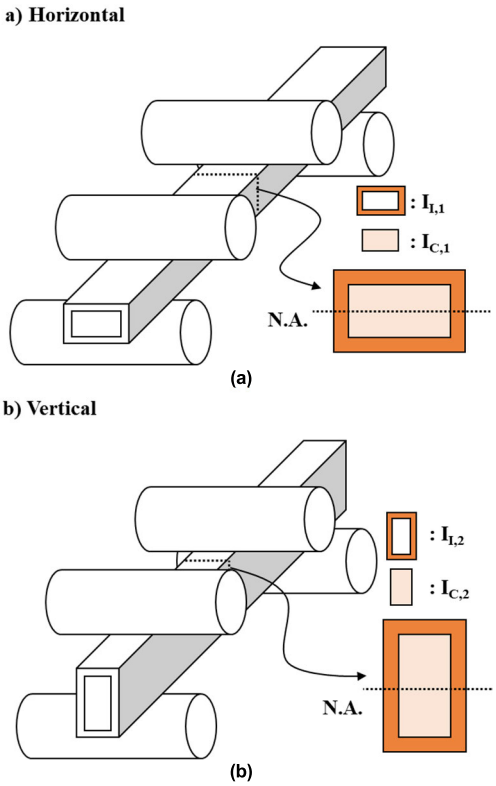

FIGURE 10. Schematic of the double-sided four-point bending test; (a) change of area moment of inertia in thickness direction and (b) area moment of inertia in vertical direction.

The proposed test method was verified through a numerical simulation. The geometry and properties of the hairpin coil mirror those employed in the tensile simulation, and the radius of each support and loading nose was set to 5 mm. As stated previously, a 3:1 ratio was employed for the distance between the supports that between the loading noses with the former set to 60 mm. The simulation results are shown in Fig. 11. Similar to the tensile simulation, most of the stress is concentrated in the copper section.

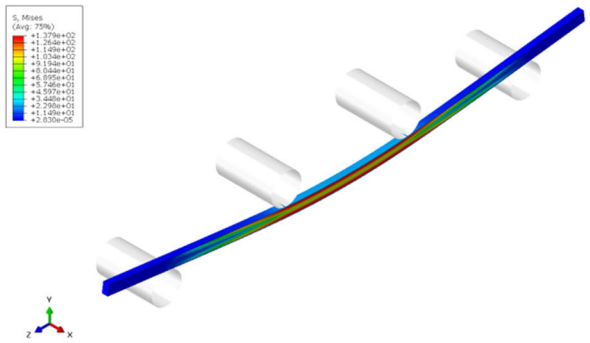

FIGURE 11. Von mises stress distribution of the four-point bending test simulation.

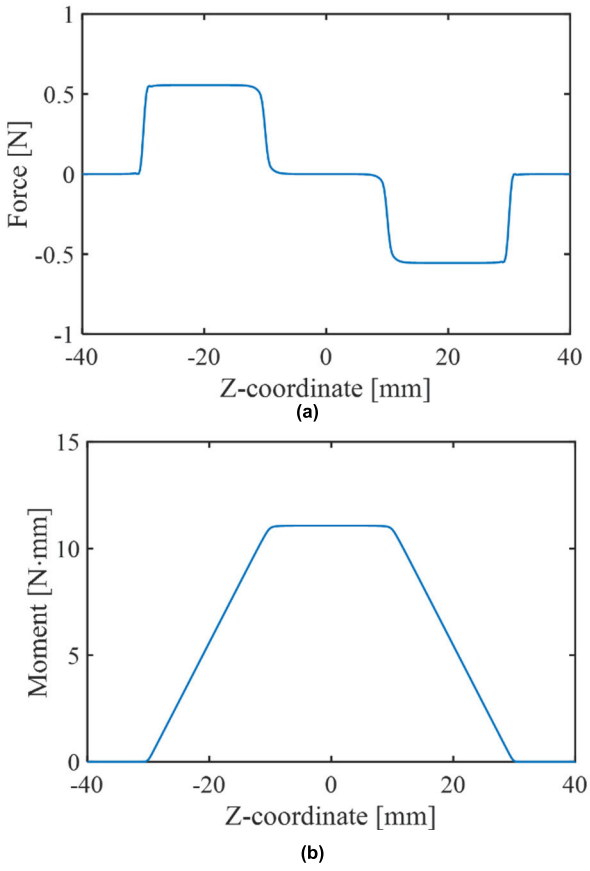

FIGURE 12. Simulation results of the four-point bending test; (a) shear force diagram and (b) bending moment diagram.

The computed results for the shear forces and bending moments of the specimens are shown in Fig. 12. The shear force has an absolute value of 0.5 N in the region outside the loading noses. Interestingly, there is zero shear force in the region between the loading

noses. This signifies that the copper-insulator composite structure of the hairpin coil remains unaffected by other force components. The bending moment exhibits a trend of linear increase and decrease outside the loading nose regions. The constant bending moment in the central region indicates that the composite structure is subjected to pure bending.

The force-deflection plot at the center of the specimen obtained from the double-sided four-point bending simulation is shown in Fig. 12. The deflection and load have a linear relationship in the elastic zone. Equation (8c) and (10b) can be employed to calculate the Young's moduli of the composite structure and individual materials from the slope and specimen dimensions. The individual Young's moduli of copper and the insulator were determined as 111.4 and 3.96 GPa, respectively, which are very close to the values directly measured in the indentation test listed in Table 1. From these values, the Young's modulus of the hairpin coil in the bending test was calculated as 87.8 GPa, which deviates from that in the tensile simulation by 3.5% error. This is considered a reasonable result and in addition, this value is close to the FE simulation and analytical calculation results listed in Table 1.

The primary analytical and numerical results in Table 2 demonstrate that double-sided four-point bending can be an alternative method for determining Young's moduli of hairpin coils. This approach allows the individual material properties to be extracted and subsequently transform into the tensile modulus of the composite structure. In the following experiments, a double-sided four-point bending test system was designed to minimize shear force and maintain a constant moment at the two loading nodes, based on the results shown in Fig. 12. The built equipment is shown in Fig. 14. Each of the subfigures show the system in different view. The span length was fixed at 60 mm for this study and the ratio of the support span length to the distance between loading noses was fixed at 3:1. The support and loading noses were fabricated with 5 mm diameters. A deflectometer that transmitted real-time data to the control PC was positioned at the center of the specimen.

An experiment was conducted using 370 mm samples at the five controlled strain rates of 10^{-2}, 5×10^{-3}, 10^{-3}, 10^{-4}, and 10^{-5} s^{-1}. These strain rates are aligned with those employed in the tensile tests, except for 10^{-1} s^{-1}. Because the bending modulus is unaffected by the specimen length, only the strain rate was considered in this experiment.

A single example of the force-deflection curve from the double-sided four-point bending test is shown in Fig. 15. Using (10b) and the slope of the force-deflection curve, the Young's moduli of copper and the insulator can be obtained. Then the Young's modulus of the hairpin can be computed from these individual moduli using (1c). The effect of strain rate on the tensile modulus calculated using the double-sided bending method is shown in Fig. 16. The consistency of the trends with those observed in the 370 mm specimen tensile tests provides further confirmation that the slope in the elastic

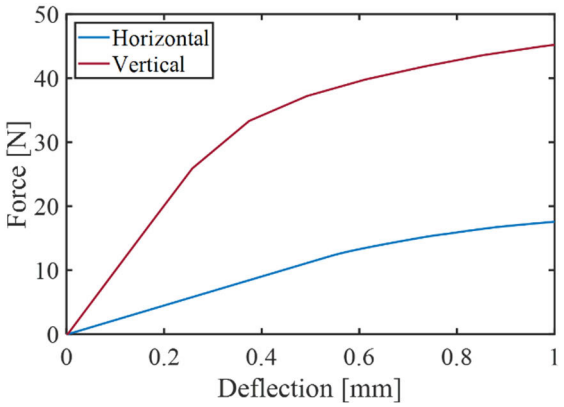

FIGURE 13. Force-deflection curve of the double side four-point bending simulation.

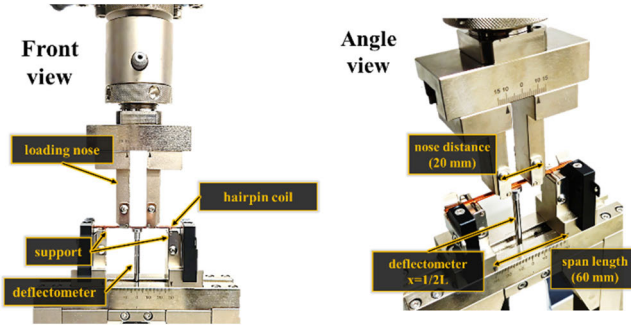

FIGURE 14. Designed four-point bending test system.

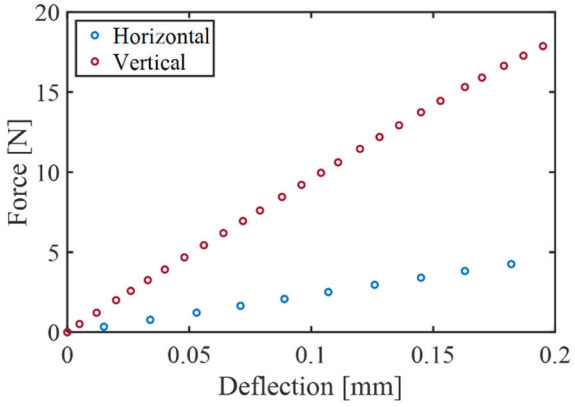

FIGURE 15. Force-deflection curve obtained from four-point bending test.

region is closely dependent on the strain rate. Notably, this response arises from the rate-dependent deformation of the material and not from any uncertainty in the instrumentation. Table 3 lists the results of the study, which show that stable values for the Young's moduli could be obtained at strain rates below 10^{-3} s^{-1}. Note that even with the same strain rate, the bending test generates only a slight deflection, making the experiment much faster.

The Young's moduli obtained from the double-sided four-point bending test at a strain rate of 10^{-4} s^{-1} of

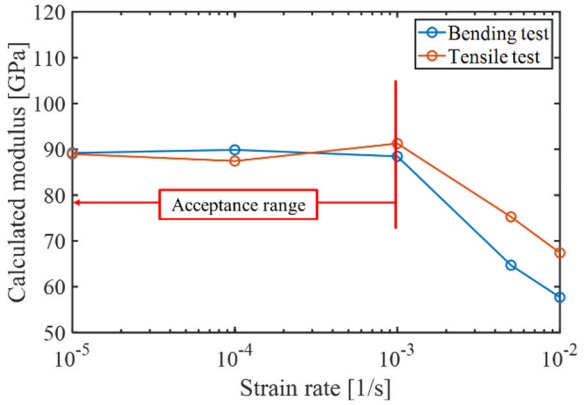

FIGURE 16. Calculated tensile moduli at different strain rates in double-sided four-point bending test.

TABLE 3. Comparison of tensile and four-point bending test based Young's modulus.

Strain rate [s^{-1}]	E_H^T [GPa]	E_H^T' [GPa]
10^{-1}	19.7	-
10^{-2}	67.4	57.7
5×10^{-3}	75.2	64.7
10^{-3}	91.2	88.4
10^{-4}	87.4	89.9
10^{-5}	89.0	89.2

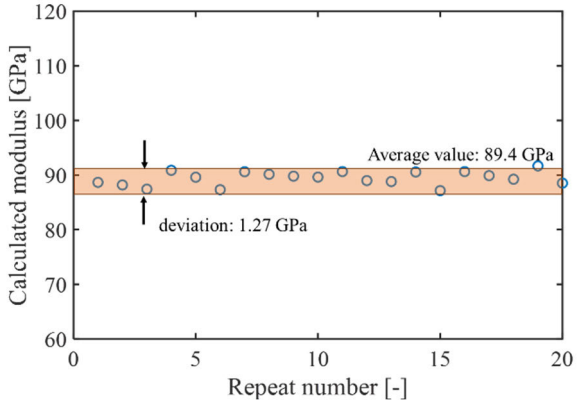

FIGURE 17. Repeatability of calculated tensile moduli from double- sided four-point bending tests.

20 tests are presented in Fig. 17. The small deviation of 1.27 GPa in the calculated tensile modulus demonstrates the excellent repeatability of the measurement. There is a negligible difference of 0.3 GPa between the average value of 89.4 GPa in the bending test and that from the tensile test under acceptable rate conditions. A notable advantage of the double-sided four-point bending test is its capability to determine the Young's moduli of individual materials without damaging the specimen. The test is explicitly targeted at ensuring a test duration of less than 10 s in the elastic range, even at the 10^{-4} s^{-1}. These advantages enable swift and precise measurements of the mechanical properties of hairpin coils in combination with conventional tensile test methods.

IV. COMBINING DOUBLE-SIDED FOUR-POINT BENDING AND TENSILE TEST

Deviations in the Young's moduli of hairpin coils measured in tensile tests significantly influences the calculation of the yield strength and springback effect. The yield strength is typically determined using the 0.2% strain offset method, which involves tracing the slope of the Young's modulus from 0.2% strain to the intersection with the stress-strain curve. Using a lower value of the Young's modulus than the actual value results in an overestimation of the yield strength. To confirm the uncertainty of the yield strength measurement by the Young's modulus variation, the experimental results of the Young's moduli according to the strain rate obtained in Sections II and III were used. The rate-dependent constant from the Johnson-Cook plasticity model (Table 1) was used to generate flow curves and evaluate the yield strength under varied strain rate conditions. Four cases were considered: a single tensile test method at 10^{-1} s^{-1}, 5×10^{-3} s^{-1}, 10^{-4} s^{-1}, and a hybrid method with a bending method at 10^{-4} s^{-1} for the elastic region and a tensile test method at 5×10^{-3} s^{-1} for the plastic region.

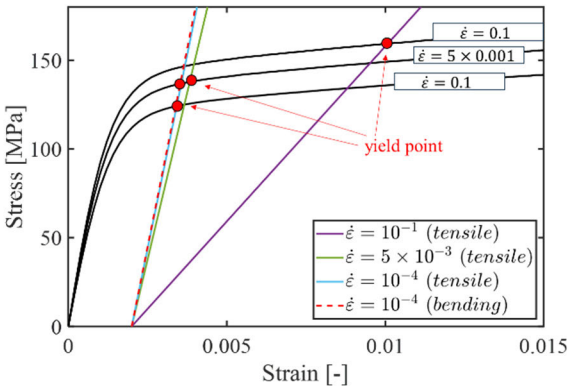

FIGURE 18. Yield point of stress-strain curve at various Young's modulus values.

TABLE 4. Comparison of yield strengths at different Young's moduli.

Experiment method	Study cases	Strain rate [s^{-1}]	σ_y [MPa]	Elastic recovery [-]
Tensile	Case 1	10^{-1}	160.0	0.00812
	Case 2	5×10^{-3}	138.1	0.00184
	Case 3	10^{-4}	123.9	0.00142
Double sided four-point bending	Case 4	10^{-4} (elastic) 5×10^{-3} (plastic)	136.8	0.00152

The yield strengths using the measured Young's moduli under different strain rate conditions are shown in Fig. 18. It is visually evident that the yield strength derived from the Young's modulus obtained at Case 1 is significantly higher than those obtained at from other strain rates. The corresponding yield strength values and recovered elastic

strain calculated using Young's moduli at different strain rates are summarized in Table 4. Specifically, the yield strength at Case 1 condition is 36.1 MPa higher than that at of Case 3. The yield strength decreased with the strain rate and ultimately converged at approximately 124 MPa. The elastic line obtained using the Young's moduli from the double-sided four-point bending test under Case 4 condition is almost coincident with that of the Case 3 and corresponds to a yield strength of 136.8 MPa. The yield strength is 12.9 MPa higher than that of Case 3. The yield strength of the hybrid method shown in Case 4 and the Case 2 shows similar yield strength due to the low hardening rate of the hairpin coil.

A notable difference arises when comparing the elastic strain recovery at the initial yield point. The inherent value of recovered elastic strain for the hairpin coil is defined as 0.00142, as demonstrated in Case 3. Despite the close values of yield strength in Cases 2 and 4, their respective elastic recoveries differ: 0.00184 for Case 2 and 0.00152 for Case 4. Consequently, the calculated errors from the defined inherent value result in 29.5% for Case 2 and 7.3% for Case 4. This will impact the effectiveness of achieving precise Young's modulus in predicting springback of the hairpin coil forming process.

V. DISCUSSION

From the calculated yield strength and elastic recovery results presented in Section IV, the results show that it is imperative to conduct the tensile test on hairpin coils at strain rates below 10^{-3} s^{-1} so that proper mechanical properties can be obtained. However, conducting tensile tests at low strain rates is time consuming and unsuitable in industrial applications. For quasi-static conditions, e.g., the total experimental time under Case 3 will cost about 4000 s when assuming the elongation of the hairpin coil is 0.4. On the other hand, experimental time can be reduced to about 100 s when conducting experiments with Case 4. Therefore, combining the double-sided four-point bending test for measuring Young's modulus and high strain rate tensile tests for the stress-strain curve determination in the plastic region is advantageous for obtaining robust mechanical properties within a short testing timeframe. However, it comes with the drawback of requiring separate jigs for each experiment and necessitating the experimenter to implement different controls for each test. Future work aims to address these by fully integrating them into a single experiment to enhance utility. Furthermore, while this study has focused on monotonic tension conditions which do not account for cycling loading properties, assessing asymmetric cycling loading properties [31], [32] with ductile fracture [33] can be considered as future work in optimization of the straightening process in hairpin coil motor manufacturing. These processes can all be fully automated through artificial intelligence technology, and they are being considered for industrial application [34], [35]. In addition, the methodology can be applied to all types of wire materials. Therefore, it is possible to generalize this approach to be applicable to a wider range of applications.

VI. CONCLUSION

This study introduces test methods to precisely measure the Young's moduli of insulated copper wires. For this purpose, this study utilized tensile tests, analytic solutions, FE simulation, and the bending method. The comprehensive conclusions drawn from this study are outlined below:

1) The Young's modulus of an insulated copper wire is essential for calculating the springback after forming. The insulator region of the wire significantly causes modulus degradation when experiments are conducted on the insulator-copper composite structure.
2) The rule-of-mixtures was used to calculate the Young's moduli of the hairpin coils in both the tensile and four-point bending tests. The analytical calculations are in good agreement with the numerical simulations. Furthermore, the Young's modulus values for each individual material (insulator and copper) can be obtained using the double-sided four-point bending test by performing the test along both vertical and horizontal directions. In this study, four-point bending test system was specifically constructed to test the insulated copper wires.
3) Tensile tests were conducted to verify the effects of the specimen length and strain rate in Young's modulus measurements. The measurement results were affected by the strain rate. The Young's modulus at a high strain rate of 10^{-1} s^{-1} had a low value of 19.7 GPa. The modulus increased to 91.2 GPa at a strain rate of 10^{-3} s^{-1}. The results from the double-sided four-point bending tests are consistent with the tensile test results.
4) The accuracy of the Young's modulus affects the calculation of yield strength of the insulated copper wires. In the 10^{-1} s^{-1} strain rate case, the calculated yield strength was 134.1 MPa, but decreased to 123.9 MPa in the 10^{-4} s^{-1} strain rate case. Therefore, the Young's modulus must be accurately measured at low strain rates below 10^{-3} s^{-1} to obtain the correct mechanical properties.
5) A low strain rate below 10^{-3} s^{-1} is recommended to reduce the variations in the tensile test results. However, this method is time-consuming, which is often undesirable in industrial applications. In this case, the double-sided four-point bending method combined with a high strain rate tensile test can be used as an alternative to reduce the test time. The use of this hybrid test method can save time and provide accurate measurements of the mechanical properties.

REFERENCES

[1] D. A. Gonzalez and D. M. Saban, "Study of the copper losses in a high-speed permanent-magnet machine with form-wound windings," *IEEE Trans. Ind. Electron.*, vol. 61, no. 6, pp. 3038–3045, Jun. 2014, doi: 10.1109/TIE.2013.2262759.

[2] G. Berardi, S. Nategh, N. Bianchi, and Y. Thioliere, "A comparison between random and hairpin winding in E-mobility applications," in *Proc. 46th Annu. Conf. IEEE Ind. Electron. Soc. (IECON)*, Oct. 2020, pp. 815–820.

[3] D.-S. Jung, Y.-H. Kim, U.-H. Lee, and H.-D. Lee, "Optimum design of the electric vehicle traction motor using the hairpin winding," in *Proc. IEEE 75th Veh. Technol. Conf. (VTC Spring)*, May 2012, pp. 1–4.

[4] M. Halwas, L. Hausmann, F. Wirth, J. Fleischer, B. Jux, and M. Doppelbauer, "Influences of design and manufacturing on the performance of electric traction drives," in *Proc. Int. Conf. Electr. Mach. (ICEM)*, Aug. 2020, pp. 488–494.

[5] T. Tóth, J. Hensel, S. Thiemer, P. Sieber, and K. Dilger, "Electron beam welding of rectangular copper wires applied in electrical drives," *Weld. World*, vol. 65, no. 11, pp. 2077–2091, Nov. 2021, doi: 10.1007/s40194-021-01158-4.

[6] A. Arzillo, P. Braglia, S. Nuzzo, D. Barater, G. Franceschini, D. Gerada, and C. Gerada, "Challenges and future opportunities of hairpin technologies," in *Proc. IEEE 29th Int. Symp. Ind. Electron. (ISIE)*, Jun. 2020, pp. 277–282.

[7] T. Glaessel, D. B. Pinhal, M. Masuch, D. Gerling, and J. Franke, "Manufacturing influences on the motor performance of traction drives with hairpin winding," in *Proc. 9th Int. Electric Drives Prod. Conf. (EDPC)*, Dec. 2019, pp. 1–8.

[8] E.-H. Lee, "A study on the effect of Young's modulus modeling on the energy conservation in elastic–plastic material computation," *Int. J. Precis. Eng. Manuf.*, vol. 21, no. 10, pp. 1875–1884, Oct. 2020, doi: 10.1007/s12541-020-00384-y.

[9] E.-H. Lee, T. B. Stoughton, and J. W. Yoon, "A new strategy to describe nonlinear elastic and asymmetric plastic behaviors with one yield surface," *Int. J. Plasticity*, vol. 98, pp. 217–238, Nov. 2017, doi: 10.1016/j.ijplas.2017.08.003.

[10] F. Wirth, C. Nguyen, J. Hofmann, and J. Fleischer, "Characterization of rectangular copper wire forming properties and derivation of control concepts for the kinematic bending of hairpin coils," *Proc. Manuf.*, vol. 47, pp. 678–685, Jan. 2020, doi: 10.1016/j.promfg.2020.04.209.

[11] A. Komodromos, C. Lobbe, and A. E. Tekkaya, "Development of forming and product properties of copper wire in a linear coil winding process," in *Proc. 7th Int. Electric Drives Prod. Conf. (EDPC)*, Dec. 2017, pp. 1–7.

[12] F. Wirth and J. Fleischer, "Influence of wire tolerances on hairpin shaping processes," in *Proc. 9th Int. Electr. Drives Prod. Conf. (EDPC)*, Dec. 2019, pp. 1–8.

[13] H. Choi, P. Fazily, J. Park, Y. Kim, J. H. Cho, J. Kim, and J. W. Yoon, "Artificial intelligence for springback compensation with electric vehicle motor component," *Int. J. Mater. Forming*, vol. 15, no. 3, May 2022, doi: 10.1007/s12289-022-01671-x.

[14] A. Riedel, M. Masuch, M. Weigelt, T. Gläßel, A. Kühl, S. Reinstein, and J. Franke, "Challenges of the hairpin technology for production techniques," in *Proc. 21st Int. Conf. Electr. Mach. Syst. (ICEMS)*, Oct. 2018, pp. 2471–2476.

[15] F. Wirth, T. Kirgör, J. Hofmann, and J. Fleischer, "FE-based simulation of hairpin shaping processes for traction drives," in *Proc. 8th Int. Electr. Drives Prod. Conf. (EDPC)*, Dec. 2018, pp. 1–5.

[16] Y. Abe, S. Semboshi, N. Masahashi, S. H. Lim, E.-A. Choi, and S. Z. Han, "Mechanical strength and electrical conductivity of Cu–In solid solution alloy wires," *Metall. Mater. Trans. A*, vol. 54, no. 3, pp. 928–938, Mar. 2023, doi: 10.1007/s11661-022-06938-1.

[17] L. Dong, F. Yang, T. Yu, N. Zhang, X. Zhou, Z. Xie, and F. Fang, "Contribution of grain boundary to strength and electrical conductivity of annealed copper wires," *J. Mater. Res. Technol.*, vol. 26, pp. 1459–1468, Sep. 2023, doi: 10.1016/j.jmrt.2023.08.012.

[18] K. Hanazaki, N. Shigeiri, and N. Tsuji, "Change in microstructures and mechanical properties during deep wire drawing of copper," *Mater. Sci. Eng. A*, vol. 527, nos. 21–22, pp. 5699–5707, Aug. 2010, doi: 10.1016/j.msea.2010.05.057.

[19] X. Li, N. Overman, T. Roosendaal, M. Olszta, C. Zhou, H. Wang, T. Perry, J. Schroth, and G. Grant, "Microstructure and mechanical properties of pure copper wire produced by shear assisted processing and extrusion," *JOM*, vol. 71, no. 12, pp. 4799–4805, Dec. 2019, doi: 10.1007/s11837-019-03752-w.

[20] P. Sun et al., "Quantitative study on the evolution of microstructure, strength, and electrical conductivity of the annealed oxygen-free copper wires," *Adv. Eng. Mater.*, vol. 24, no. 9, 2022, doi: 10.1002/adem.202200037.

[21] F. Yang, L. Dong, L. Cai, L. Wang, Z. Xie, and F. Fang, "Effect of cold drawing strain on the microstructure, mechanical properties and electrical conductivity of low-oxygen copper wires," *Mater. Sci. Eng. A*, vol. 818, Jun. 2021, doi: 10.1016/j.msea.2021.141348.

[22] F. Wirth, S. Vitzthum, J. Gerner, A. Koprivc, L. Hausmann, and J. Fleischer, "Methodology for the mechanical characterization of rectangular winding wire in the context of electric mobility," in *Proc. 13th Int. Electr. Drives Prod. Conf. (EDPC)*. Institute of Electrical and Electronics Engineers Inc., 2023, pp. 1–9, doi: 10.1109/edpc60603.2023.10372157.

[23] H. Choi, Y. Kwon, J. H. Cho, and J. W. Yoon, "Artificial intelligence-based springback compensation of EV motor component," *IOP Conf. Ser., Mater. Sci. Eng.*, vol. 1284, no. 1, Jun. 2023, Art. no. 012069, doi: 10.1088/1757-899x/1284/1/012069.

[24] H. S. Kim, S. I. Hong, and S. J. Kim, "On the rule of mixtures for predicting the mechanical properties of composites with homogeneously distributed soft and hard particles," *J. Mater. Process. Technol.*, vol. 112, no. 1, pp. 109–113, May 2001.

[25] T.-H. Kim and E.-H. Lee, "Planar reinforcement by sheet type stiffeners for fused deposition modeling," *J. Mech. Sci. Technol.*, vol. 34, no. 10, pp. 4201–4209, Oct. 2020, doi: 10.1007/s12206-020-0912-y.

[26] C. Jing, J. Wang, C. Zhang, Y. Sun, and Z. Shi, "Influence of size effect on the dynamic mechanical properties of OFHC copper at micro-/meso-scales," *Int. J. Adv. Manuf. Technol.*, vol. 120, nos. 7–8, pp. 4775–4789, Jun. 2022, doi: 10.1007/s00170-022-08674-7.

[27] E.-H. Lee, "Correlation between parameters in the microstructural vector theory and Hill's plastic potential," *Appl. Math. Model.*, vol. 124, pp. 192–215, Dec. 2023, doi: 10.1016/j.apm.2023.07.032.

[28] B. Banerjee, "An evaluation of plastic flow stress models for the simulation of high-temperature and high-strain-rate deformation of metals," 2005, *cond-mat/0512466*.

[29] Y.-D. Shim and E.-H. Lee, "An effective formability model of pearlitic steel wires in multi-stage drawing process based on the stress-based forming limit criterion," *Int. J. Precis. Eng. Manuf.*, vol. 24, no. 10, pp. 1723–1737, Oct. 2023, doi: 10.1007/s12541-022-00730-2.

[30] N. Nourmohammadi, N. P. O'Dowd, and P. M. Weaver, "Effective bending modulus of thin ply fibre composites with uniform fibre spacing," *Int. J. Solids Struct.*, vols. 196–197, pp. 26–40, Jul. 2020, doi: 10.1016/j.ijsolstr.2020.04.004.

[31] Y. Hou, J. Min, A. A. El-Aty, H. N. Han, and M.-G. Lee, "A new anisotropic-asymmetric yield criterion covering wider stress states in sheet metal forming," *Int. J. Plasticity*, vol. 166, Jul. 2023, Art. no. 103653, doi: 10.1016/j.ijplas.2023.103653.

[32] E.-H. Lee and M. B. Rubin, "Eulerian constitutive equations for the coupled influences of anisotropic yielding, the Bauschinger effect and the strength-differential effect for plane stress," *Int. J. Solids Struct.*, vol. 241, Apr. 2022, Art. no. 111475, doi: 10.1016/j.ijsolstr.2022.111475.

[33] E.-H. Lee, M. B. Rubin, J.-H. Lim, and N. Park, "A closed-form expression of a ductile fracture limit surface (FLS) for general plane stress deformation paths," *Appl. Math. Model.*, vol. 129, pp. 733–753, May 2024, doi: 10.1016/j.apm.2024.02.021.

[34] J.-S. Lee, T.-H. Kim, S.-H. Jeon, S.-H. Park, S.-H. Kim, E.-H. Lee, and J.-H. Lee, "Automation of trimming die design inspection by zigzag process between AI and CAD domains," *Eng. Appl. Artif. Intell.*, vol. 127, Jan. 2024, Art. no. 107283, doi: 10.1016/j.engappai.2023.107283.

[35] J.-H. Park, H. Park, T. Kim, J. Kim, and E.-H. Lee, "Numerical analysis of thermal and mechanical characteristics with property maps in complex semiconductor package designs," *Appl. Math. Model.*, vol. 130, pp. 140–159, Jun. 2024, doi: 10.1016/j.apm.2024.02.034.

YOUNG-DAE SHIM received the B.S. degree in mechanical engineering from Ajou University, South Korea, in 2011, and the M.S. degree in mechanical convergence engineering from Hanyang University, South Korea, in 2019. He is currently pursuing the Ph.D. degree with the Department of Smart Fabrication Technology, Sungkyunkwan University, Republic of Korea.

His research interests include the development of smart sensing systems using continuum mechanics and electromagnetic-mechanical coupled physics.

JIHUN KIM received the B.S. degree in mechanical engineering from Sungkyunkwan University, South Korea, in 2023, where he is currently pursuing the M.S. degree with the Department of Mechanical Engineering.

His research interests include multi-physics simulation and control engineering.

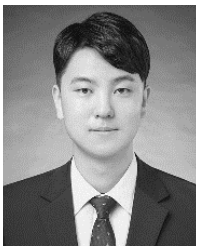

CHANGHYEON KIM received the B.S. degree in mechanical engineering from Sungkyunkwan University, South Korea, in 2021, where he is currently pursuing the combined M.S./Ph.D. degree with the Department of Mechanical Engineering.

His research interests include multi-physics simulation and signal processing.

JIHYUN PARK received the Ph.D. degree from the Department of Industrial Management and Engineering, Hanyang University, Republic of Korea, in 2019.

Since 2020, he has been a Data Scientist with Hyundai Mobis.

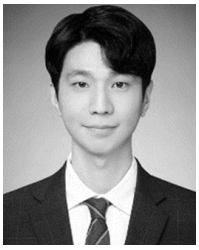

DONG-WOOK YANG received the B.S. and M.S. degrees in industrial engineering from Hanyang University, South Korea, in 2014 and 2022, respectively.

Since 2022, he has been a Data Scientist with Hyundai Mobis.

EUN-HO LEE is currently a Faculty Member with the School of Mechanical Engineering, Sungkyunkwan University, Republic of Korea. His research interests include intelligent manufacturing, semiconductor/packaging manufacturing, and multiphysics system design.